Structure Evolution during Cyclic Deformation of an Elastic Propylene-Based Ethylene−Propylene Copolymer

Shigeyuki Toki,*,† Igors Sics,† Chris Burger,† Dufei Fang,† Lizhi Liu,† Benjamin S. Hsiao,*,† Sudhin Datta,‡ and Andy H. Tsou‡

Department of Chemistry, Stony Brook University, Stony Brook, New York 11794-3400, and ExxonMobil Chemical Company, Baytown Technology & Engineering Complex-West, Baytown, Texas 77522-5200

Received January 3, 2006; Revised Manuscript Received March 17, 2006

ABSTRACT: In-situ structural evolution during uniaxial extension and subsequent retraction of a thermoplastic elastomer (TPE) based on propylene-dominant ethylene−propylene (EP) copolymer was studied. Combined measurements of time-resolved wide-angle X-ray diffraction (WAXD) and small-angle X-ray scattering (SAXS) as well as stress−strain curves revealed molecular mechanism responsible for the elastic behavior. During the first cycle of deformation, a fraction of the crystals was destroyed, while the rest was reoriented. At strains larger than 1.0, strain-induced α-crystals in the lamellar form took place, resulting in the creation of a network with well-oriented lamellae having their normals parallel to the stretching direction. With the increase of strain, more crystals were induced, forming an enhanced network with strain-hardening behavior. During retraction and even after complete relaxation to zero stress, the majority of the strain-induced crystalline network remains in tact as being "permanent set", where lamellar stacks act as the network points. This strain-induced crystalline network structure is thermally stable at room temperature and is responsible for the elastic behavior during subsequent cyclic deformation, similar to a vulcanized rubber.

Introduction

Understanding the relationships between structure and physical properties is essential for developing thermoplastic elastomer (TPE) products with elastic properties approaching those of cross-linked rubbers. Since the introduction of elastic ethylene−propylene (EP) copolymers (also referred as thermoplastic polyolefin (TPO)) in the early 1960s, this class of material has become one of the fastest growing TPEs because of its excellent ozone resistance and high extensibility, suitable to replace some vulcanized rubber goods. The typical commercialized TPOs or TPVs (i.e., vulcanized TPOs) are composed of multiple components, including polypropylene (PP), ethylene−propylene rubber (EPDM), and a substantial amount of paraffin oil. The reason why TPV can behave as a vulcanized rubber despite having the stiff PP component has been provided by Inoue et al.[1] They argued that the PP crystallites play the role of tie (cross-link) points for amorphous chains to render the elastic recovery of TPE. In other words, the fragmented crystallites behave as cross-links and the swollen amorphous PP regions behave as the rubbery domains.

Recently, Hsiao et al.[2] have studied the relationship between structure and property of an ethylene-based ethylene−propylene copolymer (made with the conventional vanadium catalyst) during tensile deformation using the time-resolved synchrotron small-angle X-ray scattering (SAXS) technique. They found that upon stretching some polyethylene crystallites were destroyed and new crystallites were induced by chain extension, resulting in the creation of a lamellar structure with its principal axis perpendicular (or its normal parallel) to the stretching direction. During retraction, strain-induced crystallites can largely remain intact with only partial relaxation of the oriented state. It is thought that the destruction of the initial PE crystals, which is often termed "mechanical melting", at relatively low strains (starting from ca. 10%) can be attributed to the high mobility of chains in the ethylene crystals.

The development of metallocene catalysis has enabled us to produce a new type of ethylene−propylene (EP) copolymer, having a polypropylene-based crystalline structure.[3−5] The metallocene reaction makes it possible to insert the ethylene unit into the polypropylene backbone randomly (not in block). The random distribution of the ethylene unit hinders the crystallization of the propylene segments. As a result, at the right composition ratio, the propylene (P)-based EP copolymer can attain a microstructure similar to the ethylene (E)-based EP copolymer[2,6−9] and other segmental elastomers such as polyurethanes[10−12] or poly(urethane−urea).[13] The propylene-based EP copolymer is considered more thermally stable (the melting point of PP is higher than that of PE) and mechanically stronger than its ethylene-based counterpart.

In this study, we investigated in-situ structure changes during cyclic uniaxial deformation of a propylene-based EP copolymer using combined synchrotron SAXS and wide-angle X-ray diffraction (WAXD) techniques. The objective of this study is to understand the molecular mechanism responsible for the elastic behavior of TPE that can be similar to vulcanized rubber. A particular emphasis was placed on the monitoring of structure evolution, involving destruction and orientation of original crystallites (e.g., mechanical melting), strain-induced new crystallites, and extension of amorphous chain segments, during the first extension and retraction cycle as well as subsequent cycles. It was found that the first cycle induced a "permanent set" crystalline network structure that dictates the resulting elastic properties.

Experimental Section

The chosen propylene-based ethylene−propylene copolymer was an experimental sample provided by the ExxonMobil Chemical

† Stony Brook University.
‡ ExxonMobil Chemical Company.
* To whom correspondence should be addressed: e-mail stoki@mail.chem.sunysb.edu, bhsiao@notes.cc.sunysb.edu; Tel (631) 632-7793; Fax (631) 632-6518.

10.1021/ma0600106 CCC: $33.50
Published on Web 04/21/2006

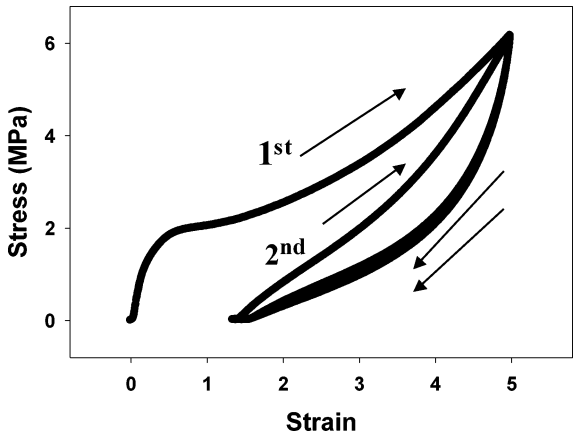

Figure 1. Stress−strain curves during extension and retraction in first and second cycles (the responses at higher ordered cyclic deformation is almost the same as that of the second cycle).

Company, having a chemical composition (84.3 wt % of the propylene content) similar to the Vistamaxx specialty elastomer. Its number-average molecular weight (M_n) was 96 000 g/mol, and its weight-average molecular weight (M_w) was 174 000 g/mol. The sample was first melt-pressed at 160 °C into a film with thickness about 1 mm, and was then rapidly quenched to room temperature in a water bath. The thermomechanical measurements of the pressed film exhibited the glass transition temperature (T_g) of −50 °C and the nominal melting temperature (T_m) of 50 °C.[3,4] The estimated crystallinity of the quenched sample was about 14%.

Time-resolved SAXS and WAXD experiments in conjunction with uniaxial tensile measurements were carried out using a modified Instron tensile apparatus[14] at the X27C beamline in the National Synchrotron Light Source (NSLS), Brookhaven National Laboratory (BNL). The wavelength used was 0.1371 nm. A MAR-CCD X-ray area detector was used for the real-time data collection. The sample-to-detector distance for WAXD was 112.6 mm and for SAXS was 1221.3 mm. The exposure time for each image was 30 s. All SAXS and WAXD images were corrected for beam fluctuations and air scattering background. In addition, the WAXD images were corrected for the effects of the curvature of the Ewald sphere using Fraser's method.[15] These corrections and further analysis were carried out using the diffraction/scattering image analysis software (POLAR) developed by Stonybrook Technology and Applied Research at Stony Brook, New York.

In the deformation study, the stretching rate was kept at 10 mm/min and the original clamp-to-clamp length was 25 mm. All measurements were performed at 25 °C. The samples were cut into a dumbbell shape. The (engineering) stress was calculated as the force (measured by the load cell) divided by the initial cross section area of the sample. The (engineering) strain was calculated as $(l - l_0)/l_0$, where l was the clamp−clamp distance during deformation and l_0 was the original sample length. Up to 10 cycles of extension/retraction uniaxial deformation were applied with the maximum strain of 5.0. The X-ray measurements were carried out in situ continuously during deformation.

The atomic force microscopy (AFM) images of the samples before and after deformation (after the second cycle of deformation) were taken by the instrument (DI-3000) from Digital Instruments. The tapping mode AFM technique was used to collect all images. Differential scanning calorimeter (DSC) measurements of the samples before and after deformation were also carried out using the DSC7 instrument from Perkin-Elmer. The samples were heated at a rate of 10 °C /min from −20 to 200 °C in an N_2 atmosphere.

Results and Discussion

The stress−strain responses of the chosen EP copolymer during extension (at strains from 0 to 5.0) and subsequent retraction in the first and second deformation cycles are shown in Figure 1. This sample possessed the ability of large extension with a maximum elongation-to-break ratio greater than 6.0.[3,4] In the first cycle, the stress−strain curve during extension exhibited no apparent yield point. However, a break point at a strain about 0.5, above which the rate of stress increase significantly decreased, was seen. This break point is associated with the "permanent set" behavior, which will be discussed later. The recovery strain at the zero stress was about 1.2. In the second cycle, the sample exhibited an excellent elastic behavior, i.e., no yield stress and no further permanent set behavior, similar to a vulcanized natural rubber. In fact, the stress−strain responses in the third and higher cycles (data not shown) were nearly identical to those of the second cycle. It is clear that the permanent set behavior is induced by the first cycle deformation at strain around 1.0, which is relatively small compare to the maximum applied strain but significantly larger than that of the ethylene-based EP copolymer (ca. strain at 0.1).[2] Hereafter, only the structure changes in the first and second cycles are discussed, as those in the higher cycles are identical to those in the second cycle.

Structural Changes during the First Deformation Cycle. *WAXD Results.* The stress−strain curves and selected WAXD patterns (each image was taken at the strain indicated by the arrow) during extension up to strain 5.0 and subsequent retraction back to strain 1.7 (i.e., at zero stress) in the first deformation cycle are shown in Figure 2. At strain zero, an isotropic broad amorphous halo superimposed with a sharp crystal reflection ring ((040) reflection from the α-form) was observed in the corresponding WAXD pattern. The crystal reflection ring suggested the existence of randomly distributed crystals created in the quenching process during molding. It was seen that during extension this isotropic (040) crystal ring was first transformed into two arcs and then two distinct spots on the equator. At strains ≥3.0, two additional equatorial reflection peaks ((110) and (130)) also appeared, representing the existence of oriented α-form crystals.

To analyze the WAXD image quantitatively, we adopted the following procedure to evaluate the mass fractions of oriented crystal, unoriented crystal, oriented amorphous, and unoriented amorphous phases. In this procedure, the 2D image collected in the flat-plate geometry (by a CCD area detector) was transformed into an undistorted geometry in reciprocal space using the procedure described by Fraser et al.[15] The missing data in the meridional region were estimated using the expansion of Legendre polynomials:[14]

$$I(s,\phi) = \sum a_{2n} P_{2n}(\cos\phi) \tag{1}$$

with $s = 2\sin(\theta/2)/\lambda$, ϕ being the azimuthal angle, P_{2n} being the Legendre polynomial of the first kind of order n, and a_{2n} being the fit coefficient. The diffraction intensity of the 2D pattern was subsequently integrated cylindrically to obtain the linear intensity profile $I(s)$

$$I(s) = \int I(s,\phi)\sin\phi\, d\phi \tag{2}$$

Figure 3 illustrates an example WAXD profile integrated cylindrically at strain 5.0. A peak fitting program was used to deconvolute this profile and yielded the amorphous background and corresponding crystal diffraction peaks: (110) at $s = 1.59$ nm^{-1}, (040) at 1.91 nm^{-1}, (130) at 2.09 nm^{-1}, and (111) at 2.41 nm^{-1}, for the α-form structure of iPP.[16−18] All crystalline and amorphous peaks were described by the Voigt functions. The crystalline fraction (or amorphous fraction) was calculated as the ratio of the total area of crystal peaks (or amorphous peak) to the total area underneath the diffraction profile. The

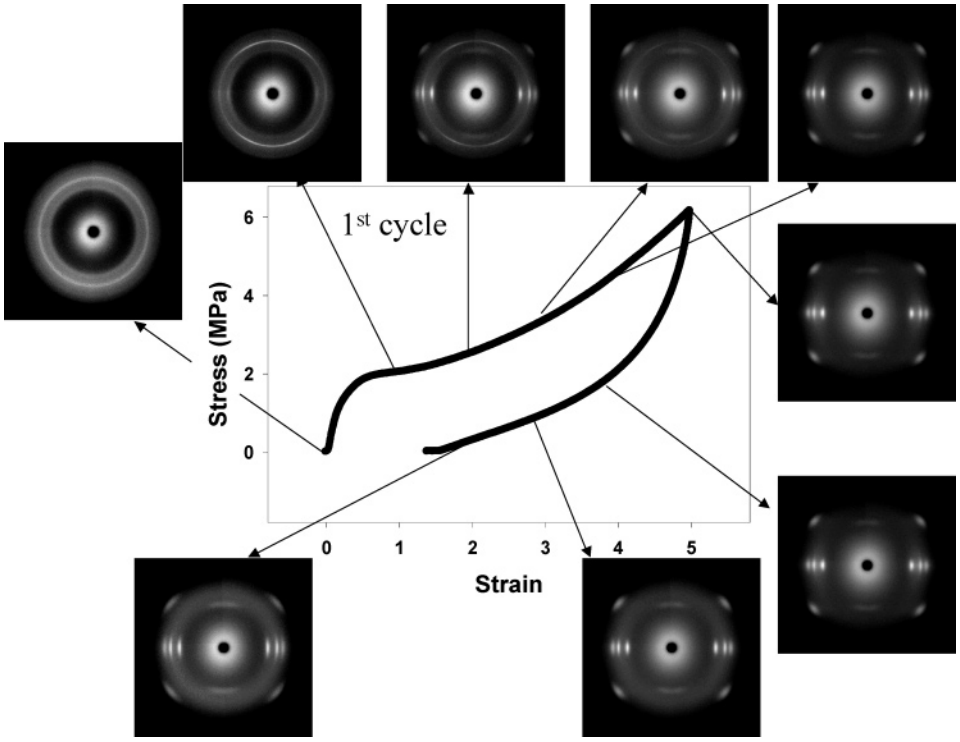

Figure 2. Stress−strain curves and selected WAXD patterns during extension and retraction in the first cycles. Each image was taken at the average strain indicated by the arrow.

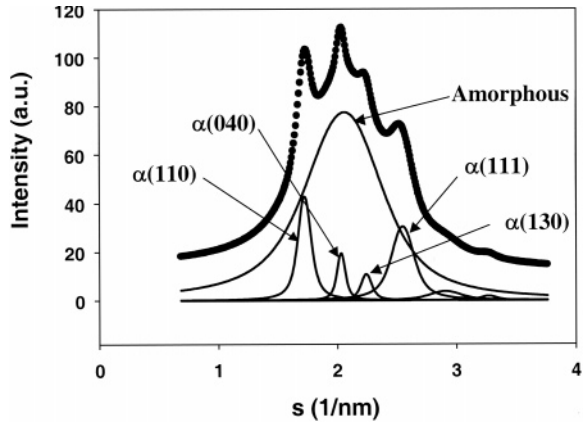

Figure 3. Deconvolution of an integrated intensity profile for calculation of the amorphous and crystalline fractions from the Fraser-corrected[15] 2D WAXD pattern using eq 2 at strain 5.0 in the first cycle

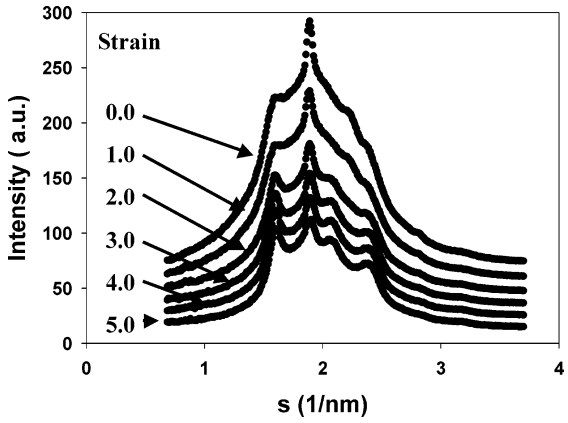

Figure 4. Integrated intensity profiles (from the Fraser-corrected[15] 2D WAXD patterns) at various strains as a function of scattering vector *s*.

crystalline fraction (I_C) can be further divided into two fractions: oriented crystal (I_{OC}) and unoriented crystal (I_{UC}) fractions as follows:

$$I_C = I_{OC} + I_{UC} \tag{3}$$

The oriented crystal fraction is directional dependent and is associated with the deformed region of crystallized chains; the unoriented crystal fraction is directional independent and is associated with the undeformed region of crystallized chains. To evaluate the contributions of I_{OC} and I_{UC} separately, the scattering profiles at the meridian and equator were deconvoluted.[11,12] The scattered intensity at the meridian (I_M) consists of contributions from both unoriented crystal and unoriented amorphous (I_{UA}) phases.

$$I_M = I_{UC} + I_{UA} \tag{4}$$

The scattered intensity at the equator (I_E) consists of contributions from oriented crystal, oriented amorphous, unoriented crystal, and unoriented amorphous phases.

$$I_E = I_{OC} + I_{OA} + I_{UC} + I_{UA} \tag{5}$$

The evaluation of I_C, I_M, and I_E from the 2D WAXD profile makes it possible to determine all four components: I_{OC}, I_{OA}, I_{UC}, and I_{UA}.

The integrated scattered intensities using eq 2 at different strains during extension are shown in Figure 4. It is clear that the undeformed initial sample (at strain zero) possessed a relatively low degree of crystallinity about 14% with an intense (040) peak. Upon deformation, all other diffraction peaks intensified, indicating the increase of crystallinity as well as the crystal perfection. However, the basic crystal structure was not changed (i.e., the α-form) during extension since the diffraction peak positions remained at the same locations. Using

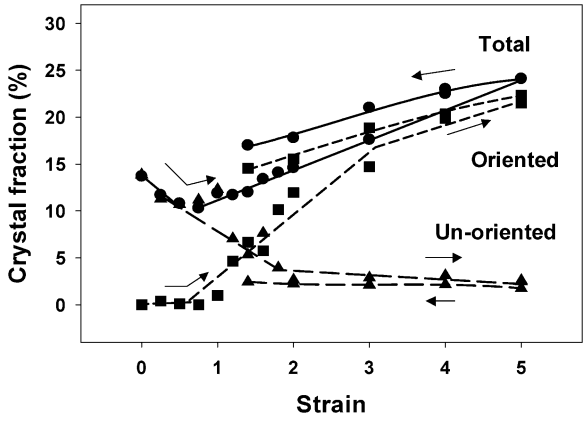

Figure 5. Fractions of total crystal, oriented crystal, and unoriented crystal phase at varying strains during extension and retraction in the first cycle.

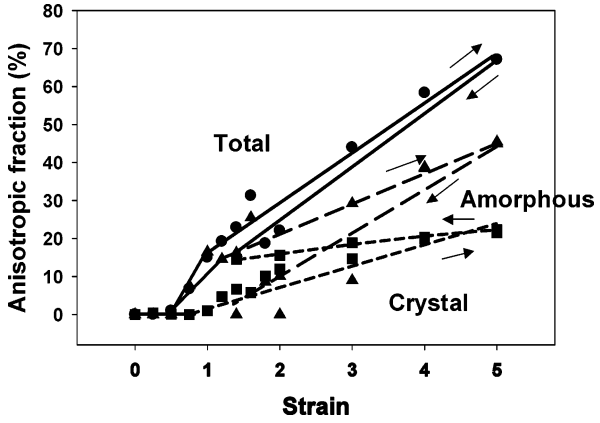

Figure 6. Fractions of total anisotropy, oriented amorphous, and oriented crystal phases at varying strains during extension and retraction in the first cycle.

the procedures outlined in eqs 3−5, all four mass fractions—I_{OC}, I_{OA}, I_{UC}, and I_{UA}—were calculated.

The total crystal fraction, oriented crystal fraction (I_{OC}), and unoriented crystal fraction (I_{UC}) during extension and retraction are shown in Figure 5. At strain zero, the total crystal fraction was the same as the unoriented crystal fraction, which was about 14%, and both values decreased with strain. This indicates that a fraction of the original crystals was destroyed at the initial deformation stages. At strain 0.7, the total crystal fraction decreased about 4% (from 14% to 10%); at strains above 0.7, both total crystal fraction and oriented crystal fraction increased with strain, indicating the occurrence of strain-induced crystallization, whereas the unoriented crystal fraction decreased continuously with strain. The increase of the total crystal fraction was slower than that of the oriented crystal fraction, suggesting that some unoriented crystals were reoriented by extension. It is interesting to note that (1) at strain 5.0 the total crystal fraction increased to 25%, i.e., a 15% increase due to strain-induced crystallization, and (2) the unoriented crystal fraction did not return to 0% (i.e., completely vanish). In fact, the decrease in unoriented crystal fraction exhibited a two-stage process: at strains between 0 and 1.9, the unoriented crystal fraction decreased at a fast rate (from 14% to about 4%); at strains between 1.9 and 5.0, the unoriented crystal fraction decreased at a slow rate (from 4% to 2.5%). During retraction, the fraction of the unoriented crystal increased very slightly (2.5% to 3.5%), while both total crystal fraction and oriented crystal fraction decreased notably. For example, at strain 1.7, where the stress returns to zero, the total crystal fraction was about 17%, i.e., an 8% decrease from strain 5.0. This indicates that a small fraction of strain-induced crystallites is not thermally stable under the unstrained state at room temperature, since they melt away upon relaxation. However, the majority of the strain-induced crystallites are thermally stable, and they form a network structure and can be considered as being permanent set.

The anisotropic fractions of total, oriented amorphous, and oriented crystal phases during extension and retraction are shown in Figure 6. The total anisotropic fraction exhibited a distinct transition at strain 0.7, above which the value began to increase rapidly from 0 to about 20% at strain 1.0. This can be attributed to the reorientation of some original crystals. At strains larger than 1.0, the total anisotropy, fractions of oriented amorphous and crystalline phases all increased with strain in a nearly linear fashion. The final level of the total anisotropy in the chosen TPE was found to be much higher than the value observed in vulcanized rubber.[19−21] The difference may be due to the shorter average molecular weight (M_n) in the amorphous region of the TPE than that of typical cross-linked rubber, since rubber usually has a heterogeneous distribution of cross-link points[19] with an average molecular weight between the cross-links larger than 100 000 g/mol. The highly oriented amorphous fraction means that the non-Gaussian chains between network points are extended and can significantly increase the entropy stress. During retraction, the fraction of oriented amorphous phase decreased to zero at zero stress, while the fraction of oriented crystal decreased only slightly and remained at a finite value (ca. 15%). It is thus suggested that the extension of the amorphous molecules is mainly responsible for the observed stress upturn, not the orientation of the crystal phase.

SAXS Results. To investigate the change of lamellar structure in TPE during deformation, in-situ small-angle X-ray scattering (SAXS) experiments were also carried out. During the extension and retraction processes in the first cycle, the stress−strain relationship and selected SAXS patterns are shown in Figure 7. Each image was taken at the average strain indicated by the arrow. During extension, the SAXS image changed from a circular pattern (at strain < 0.7), to a $(4 + 2)$-point pattern (four scattering peaks on the two off-axes and two scattering peaks on the meridian, at strain between 0.7 and 1.0), and then to a 2-point pattern (two scattering peaks on the meridian, at strain > 1.0), which are consistent with the WAXD results. Upon retraction, the image changed from a 2-point pattern to a 4-point pattern (four scattering peaks on two off-axes). The circular pattern represents the existence of randomly oriented lamellar stricture, where the 2-, 4-, and $(2 + 4)$-point patterns indicate the transformation and the reorientation of the lamellar structure during extension.

The quantitative analysis of the SAXS pattern in terms of the centers, widths, intensities, and tilt angles for all discrete scattering peaks can be carried out using the following procedure. A factorized fit function $f(x,y)$ with the combination of Gaussian and Lorentzian distributions can be used to describe each scattering peak in either the 2-point, 4-point, or $(2 + 4)$-pattern. The analysis of a typical 4-point pattern is illustrated as follows. The symmetry of the 4-point SAXS pattern (in reciprocal space) against the $x-y$ axes and its relationship with the arrangement of a lamellar assembly (in real space) are

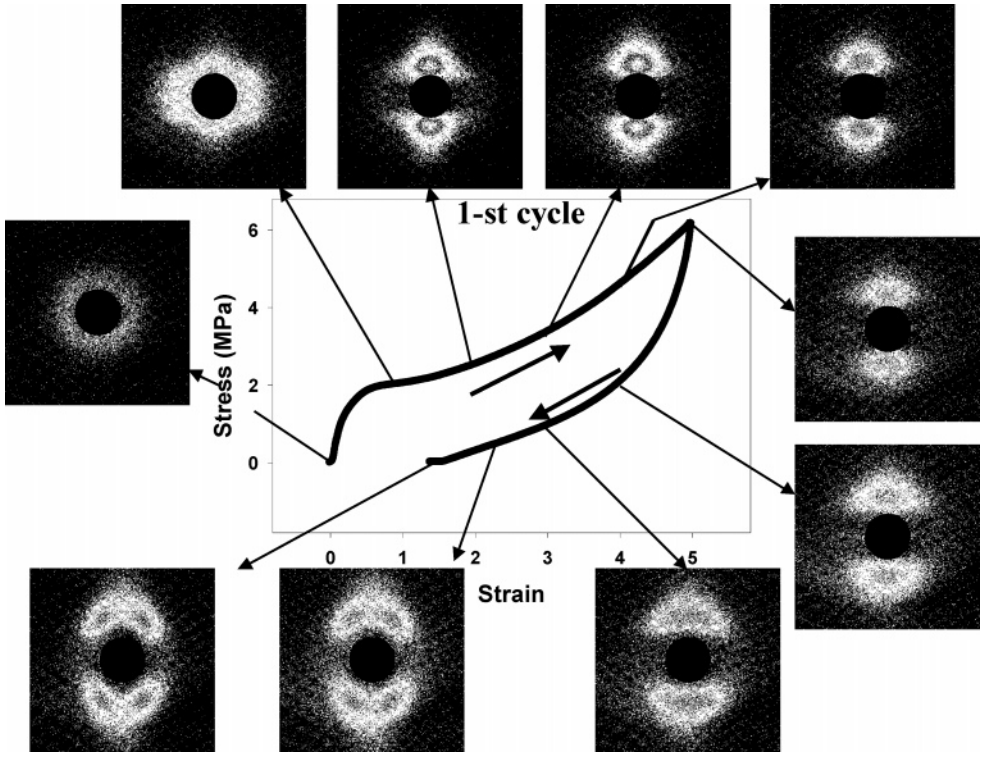

Figure 7. Stress−strain curves and selected SAXS patterns during extension and retraction in the first cycles. Each image was taken at the average strain indicated by the arrow.

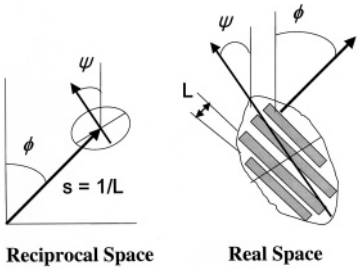

Figure 8. Relationships between the scattering pattern in reciprocal space and the lamellar assembly (stack) in real space (s = scattering vector, L = long period, ϕ = the angle of each lamella in the stack with respect to the stretching direction, ψ = the angle of the lamellar stack in the microstructural arrangement with respect to the stretching direction).

illustrated in Figure 8, where the following relationships can be established.

$$P_1(x) = 1.0/(1.0 + \pi^2 x^2) \quad (6)$$

$$P_2(x) = \exp(-\pi x^2) \quad (7)$$

$$f_1(x,y) = P_2((x\cos\psi + y\sin\psi)/wx)\, P_1((-x\sin\psi + y\cos\psi)/wy) \quad (8)$$

$$f_2(x,y) = P_2((x\cos\psi - y\sin\psi)/wx)\, P_1((-x\sin\psi + y\cos\psi)/wy) \quad (9)$$

$$f(x,y) = (f_1(x - x_0, y - y_0) + f_2(x + x_0, y - y_0) + f_2(x - x_0, y + y_0) + f_1(x + x_0, y + y_0))/(x^2 + y^2) \quad (10)$$

In Figure 8, the long period of the lamellar assembly, L, is related to the scattering vector, s (= $1/L$), of the scattering maximum in reciprocal space. The angle of each lamella in the assembly (i.e., lamellar stack) with respect to the stretching direction is defined as ϕ, where the angle of the lamellar stack in the microstructural arrangement with respect to the stretching direction is defined as ψ. The values of ϕ and ψ are thus affected by the orientation distributions of the individual lamella and the lamellar stacks, respectively. The schematic diagrams of the simulated scattering patterns (by Fourier transformation) based on different lamellae and lamellar stack arrangements (at different ϕ and ψ) are shown in Figure 9. These diagrams have been illustrated by Bonart et al. before.[22] Recently, SAXS studies on poly(urethane−urea) (Lycra) elastomer[23] and ethylene-based EP elastomers[2] showed similar morphological changes under deformation. In Figure 10, in the scenario of a fixed angle for the lamellar stack at $\psi = 30°$ (the left side of Figure 10), the variation of the angle for the lamella with respect to the stretching direction at $\phi = 30°$ and $-30°$ creates 4-point patterns of opposite shape and $\phi = 0°$ creates a 2-point pattern. On the other hand, at the fixed angle $\phi = 0°$, the variation of ψ at 30°, 0°, and −30° creates 2-point patterns. Therefore, it is logical to conclude that the 4-point pattern observed in this study is caused

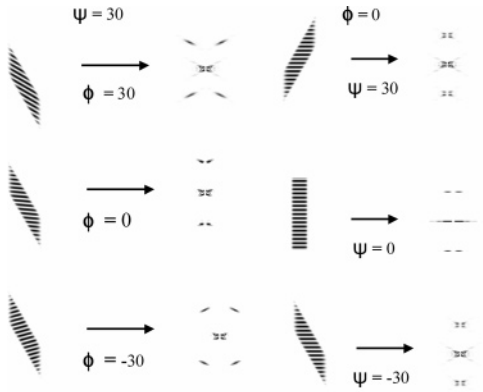

Figure 9. Relationships between the lamellar stacks with different spatial arrangements (i.e., different ϕ and ψ) and simulated SAXS patterns.

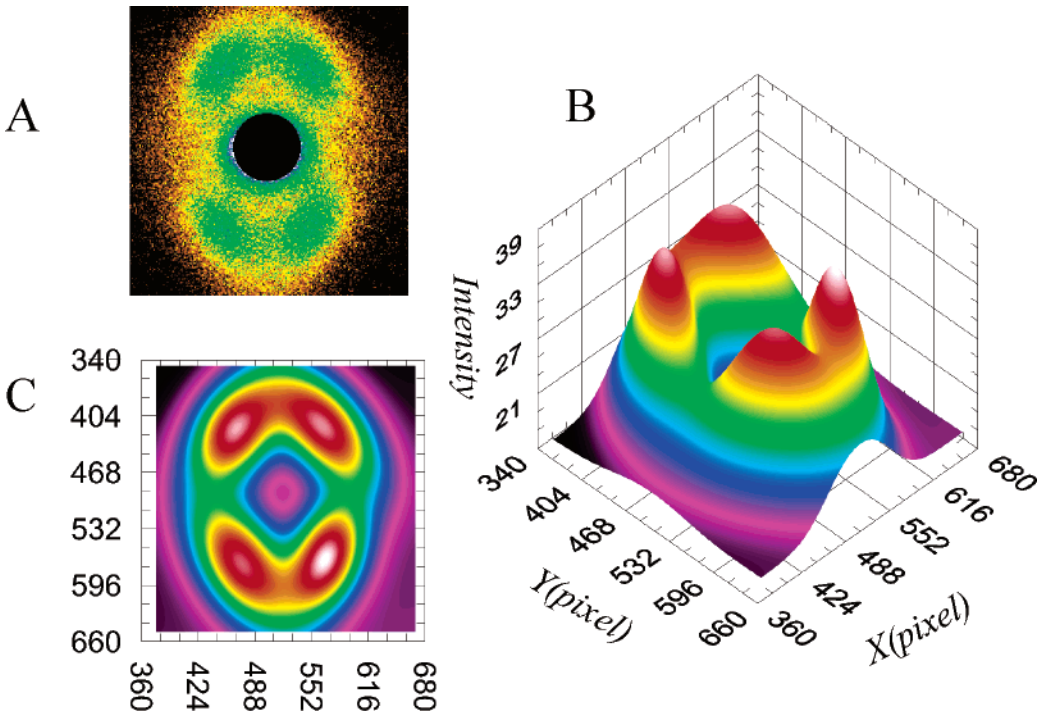

Figure 10. (A) Experimental SAXS pattern, (B) 3-dimensional fitting SAXS profile using eq 10, and (C) top view of the fitting SAXS profile.

by the tilting of the lamellae against the stretching direction within the lamellar stacks, as illustrated in the bottom left diagram in Figure 9, whereas the 2-point pattern can be described by the lamellar arrangements without tilting (e.g., $\phi = 0°$). The (2 + 4)-point pattern may represent the sum of two lamellar populations: one with tilted lamellae and one with nontilted lamellae.

The experimental SAXS data can be quantitatively fitted using the mathematic functions based on eq 10. For example, an example 4-point pattern was analyzed using the nonlinear iterative fitting procedure with these functions, and the results are illustrated in Figure 10 (A, the measured SAXS pattern; B, the 3-dimensional fitting SAXS profile; and C, the top view of the fitting SAXS profile). It is clear that the experimental data and the top view of the fitted result showed an excellent match. From the fitted functions, one can determine the peak centers, their widths, and the oblique angles of corresponding orientations for lamellae and lamellar stacks. The position of the scattering peak in reciprocal space corresponds to the inverse of the long spacing in real space, and the angle of the peak with respect to the stretching direction corresponds to the orientation of lamellar stack assembly. The lamellar stack morphology is consistent with the distinct scattering peaks even though the crystallinity is relatively low (the maximum crystallinity under the strained condition is around 25% and under the relaxed condition is around 15%).

The fitted results of all measured SAXS patterns during extension and retraction revealed a very large body of structure parameters. Two major conclusions can be drawn from these results. (1) During deformation, two discrete populations of lamellar arrangements—the population with tilted lamellae and the population with the lamellar normal parallel to the stretching (machine) direction—can be produced, depending on the applied strain in the extension or retraction process. The population with the lamellar normal parallel to the stretching direction is the dominant population at high strains. It is most affected by the applied stress and thus is largely responsible for the mechanical response during deformation. (2) The most insightful structure

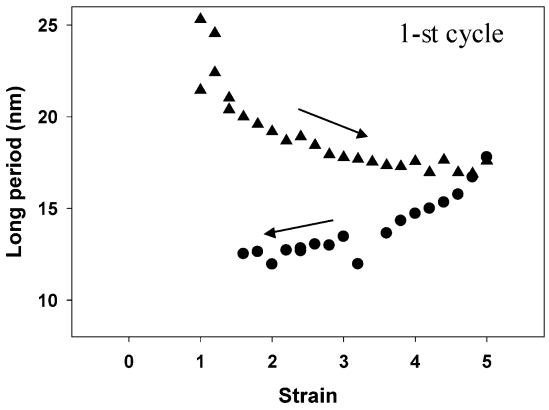

Figure 11. Change of long period L from the major lamellar population with strain during extension and retraction in the first cycle.

parameter is the long period of the dominant lamellar population, which can also be calculated directly from the position of the most intense scattering peak, as described in the general literature. The relationship between the long period L of the dominant lamellar population and the applied strain during extension and retraction in the first cycle is shown in Figure 11. In this figure, the values of L below strain 1.0 were omitted because results were so fluctuated that the experimental uncertainty was too high to be meaningful. These fluctuations are due to the process of mechanical melting, which will be discussed later. It was found that the value of L decreased with strain during extension. This is a very interesting behavior because the distance in the material usually extends with increasing strain under normal stretching conditions. However, the observed feature is due to a different behavior, i.e., strain-induced crystallization. On the basis of the WAXD results (Figure 5), it is clear that the crystal fraction is increased during extension. As the strain-induced crystalline lamellae most likely occur in the stretched and orientated amorphous regions between existing lamellae, the process would decrease the average long spacing between the lamellae during extension. This peculiar behavior has also been reported in ethylene-based ethylene−

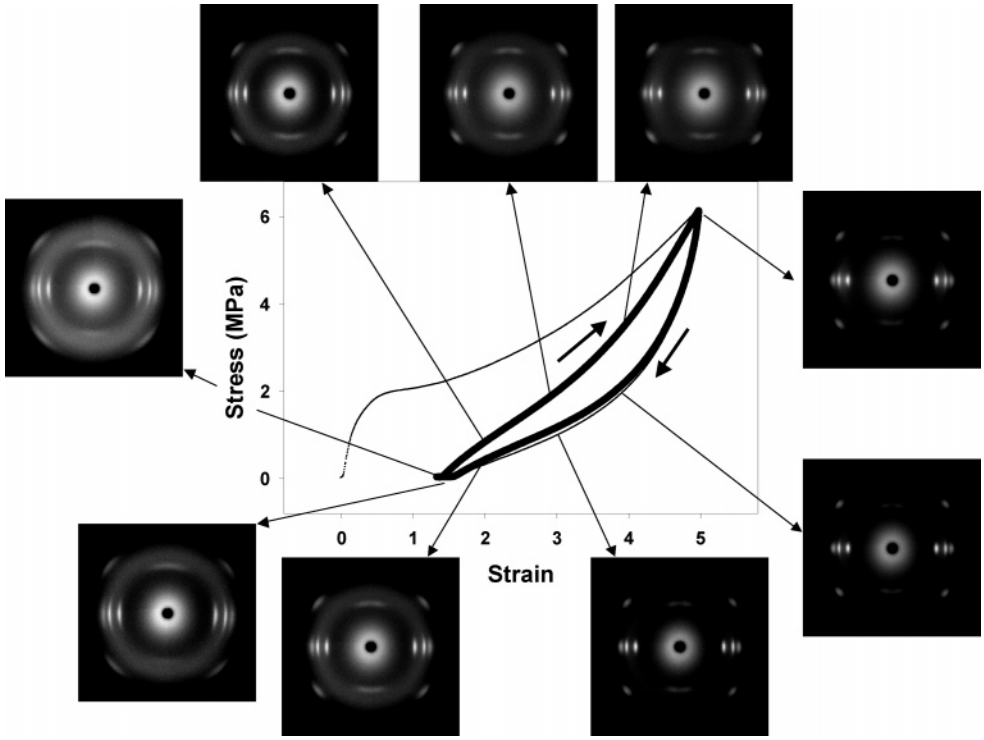

Figure 12. Stress−strain curves and selected WAXD patterns during extension and retraction in the second cycle. Each image was taken at the average strain indicated by the arrow.

propylene copolymer recently.[2] During retraction, L was found to further decrease with decreasing strain. This is due to the relaxation behavior of the permanent set crystalline lamellar network instead of the further crystallization process. In contrast, some portions of defective crystals were melted away during retraction, but which did not affect much on the average distance between the lamellae in the major lamellar population.

Structural Changes during the Second Deformation Cycle. During the extension and retraction processes in the second cycle, the stress−strain relationship and selected corresponding WAXD patterns are illustrated in Figure 12. Each WAXD image was taken at the average strain indicated by the arrow. The stress−strain relationship of the once-stretched TPE (to the maximum strain of 5.0) was completely reversible at higher ordered cycles (data not shown), exhibiting near identical curves with a small hysteresis loss and no yield stress. The mechanical behavior of the permanent set TPE after the first cycle is very similar to that of the cross-linked rubber. In the second cycle, the WAXD patterns also seemed to be reversible. During extension, the WAXD patterns exhibited a distinct increase of the crystal fraction, whereas during retraction, the patterns indicated a decrease of the crystal fraction.

The crystalline fractions (total, oriented, and unoriented) at each strain during extension and retraction are shown in Figure 13. It was seen that both the total crystal fraction and the oriented crystal fraction all increased during extension and decreased during retraction. The unoriented crystal fraction, however, only slightly decreased during extension and increased during retraction. This behavior is similar to that of cross-linked rubber, which suggested that the strain-induced crystals in the second cycle (or the high ordered cycles) are completely oriented; these crystals are not thermally stable and can melt away upon relaxation at room temperature. In contrast, the crystalline network after permanent set by the first deformation cycle is quite stable at room temperature. Although the strain-induced

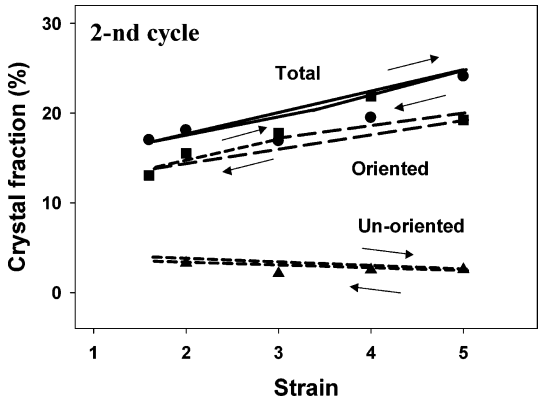

Figure 13. Fractions of total crystal, oriented crystal, and unoriented crystal at varying strains during extension and retraction in the second cycle.

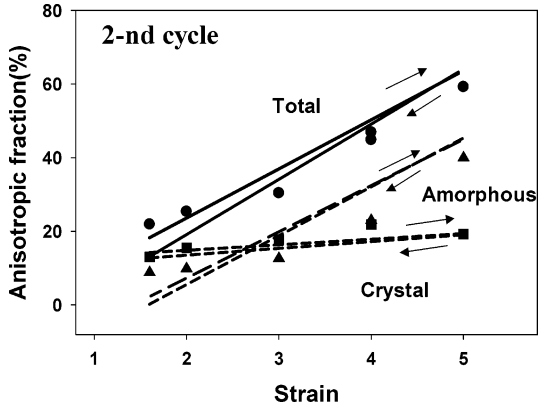

Figure 14. Fractions of total anisotropy and oriented amorphous and oriented crystal phases at varying strains during extension and retraction in the second cycle.

crystals appear to be defective (e.g., fringe-micelle-like) and small, their presence clearly increases the total network points and enhances the overall stress (i.e., strain hardening).

CDV

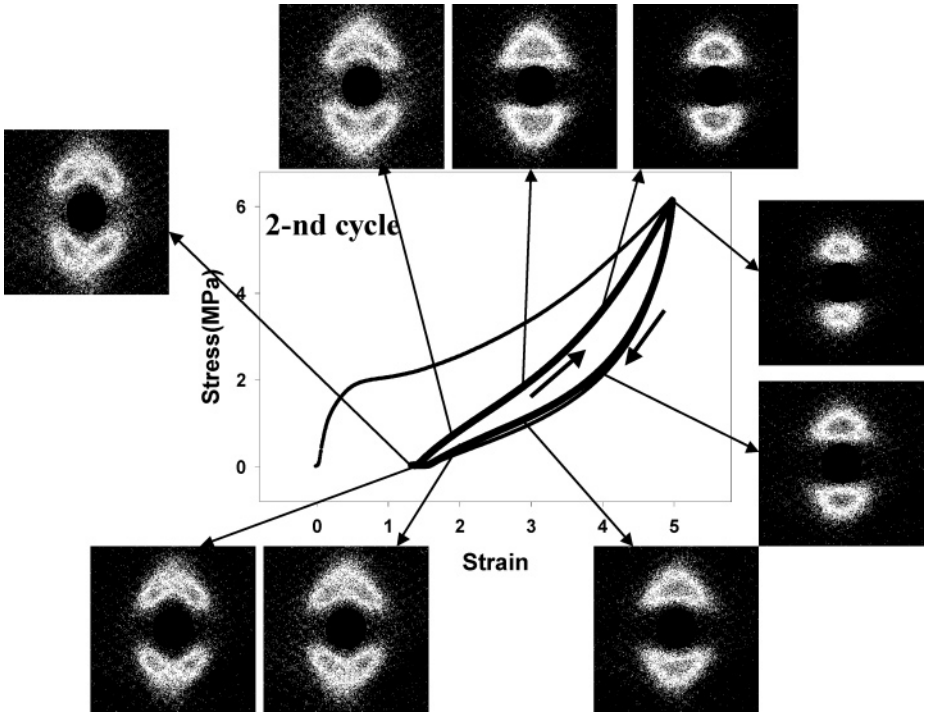

Figure 15. Stress−strain curves and selected SAXS patterns during extension and retraction in the second cycle. Each image was taken at the average strain indicated by the arrow.

The anisotropic fractions of total, oriented amorphous, and oriented crystal phases during extension and retraction in the second cycle are illustrated in Figure 14. It was seen that all three fractions (total, oriented amorphous, and oriented crystal) increased with strain during extension and decreased upon retraction. However, the increase of the oriented amorphous fraction was significantly larger than that of the oriented crystal fraction and dominated the increase of the total anisotropic fraction. This result can explain the observed elasticity behavior of the TPE after being permanent set, where the stress upturn can be mainly attributed to the entropy reduction of the amorphous chain segments between the network points.

The relationships between the stress−strain curves and selected corresponding SAXS patterns during the extension and retraction processes in the second cycle are shown in Figure 15. It was seen that the SAXS profile changed from a 4-point pattern to a 2-point pattern during extension and from a 2-point pattern back to a 4-point pattern during retraction. As discussed earlier, the 4-point pattern indicates the tilting of lamellae in the lamellar stacks, where the 2-point pattern suggests that the lamellar normal becomes parallel to the stretching direction. The observed SAXS pattern changes thus indicated the simultaneous processes of lamellar reorientation (its normal becomes aligned with the stretching direction) and strain-induced crystallization during extension and the reversed processes of lamellar tilting and relaxation-induced melting upon retraction. These events are reversible at room temperature.

The long period values from the dominant lamellar population at different strains during extension and retraction in the second cycle are shown in Figure 16. It was seen that the average long period L increased with strain during extension and decreased during extraction. These results are directly related to the structure changes in the network points (i.e., lamellar stacks) from the dominant lamellar population, which is thermally stable but deformable under deformation. The changes include the slightly separation of lamellae in the stacks and the reorientation of the lamellae having their normals parallel to the stretching

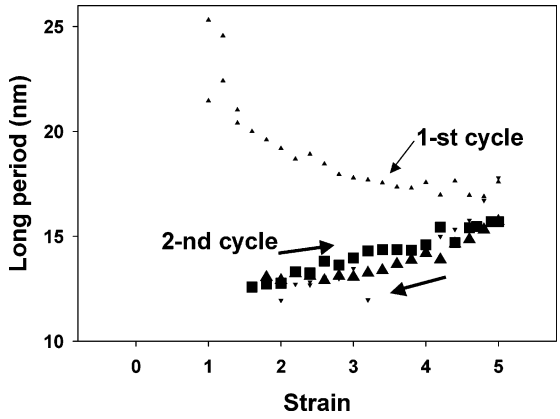

Figure 16. Change of the long period L from the major lamellar population with strain during extension and retraction in the second cycle (small triangles represent the values in the first cycle).

directions. Upon relaxation, the lamellae in these network points (stacks) contract and become tilted. However, the slight compliance in the structure of the network points (lamellar stacks) does not affect the near ideal rubber elasticity of the permanent set TPE.

Permanent Set of the Crystalline Network Structure for Elastic Behavior. The process of mechanical melting during tensile deformation in semicrystalline polymers has been well documented,[24] and it also takes place during extension of TPE at the low strain region in the first cycle (as seen in Figure 5). This process is essential for creating a permanent set network of amorphous tie chains connecting the adjacent lamellar stacks (cross-link points).

The process of lamellar rearrangement has been confirmed by the AFM measurement (in tapping mode) on the TPE samples before and after deformation, which are shown in parts A and B of Figure 17, respectively. The AFM image of the sample before deformation exhibited the existence of lamellar structure in the spherulitic arrangement without preferred orientation. However, the AFM image of the sample after

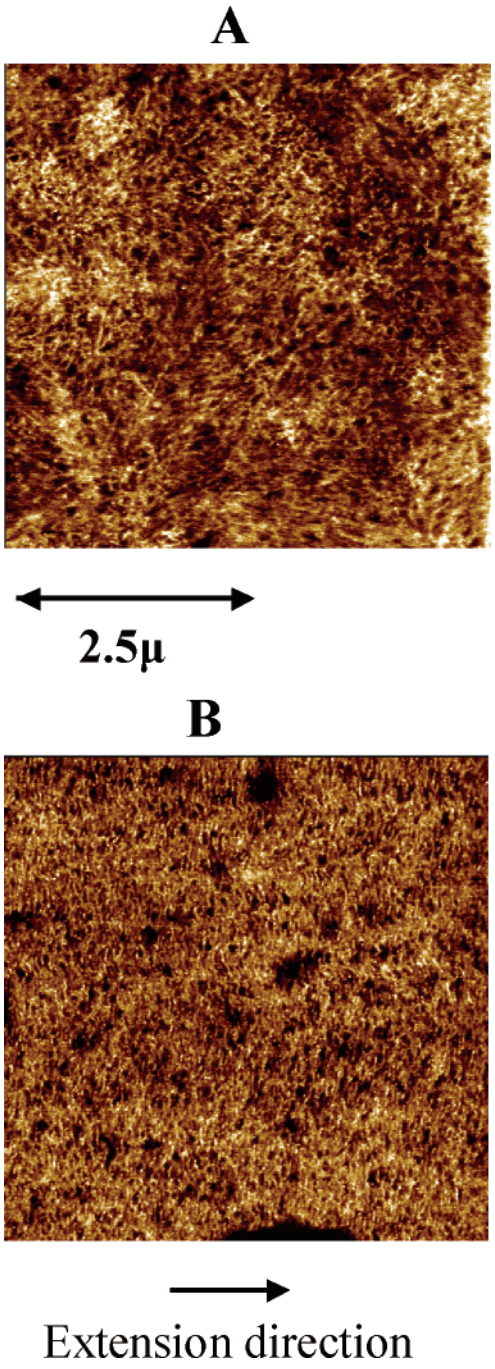

Figure 17. AFM images of the TPE sample (A) before deformation and (B) after deformation.

deformation clearly showed an oriented lamellar structure having the lamellar normal parallel to the stretching direction.

On the basis of experimental results in this study, one can propose several schematic diagrams shown in Figure 18 to illustrate the permanent set mechanism during the deformation of TPE in the first cycle. Diagram A indicates the sample before deformation, having folded-chain lamellae without any preferred orientation. Diagram B indicates that during extension below strain 1.0 some original crystallites are destroyed and new crystallites with thinner thickness (this was confirmed by the DSC, where the undeformed sample exhibited a melting peak of 48.0 °C and the deformed sample showing the melting peak of 43.7 °C) are developed. These strain-induced thinner lamellae are probably fringe-micelle-like without the folded-chain conformation. The process of permanent set is probably completed

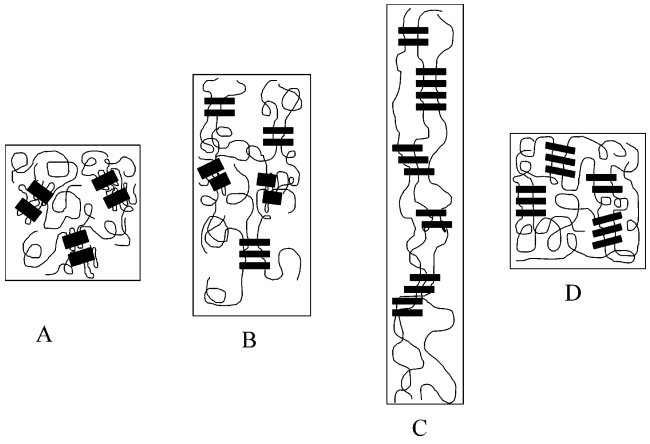

Figure 18. Schematic diagrams to illustrate the permanent set mechanism during extension and retraction in the first cycle: (A) before deformation, (B) during extension below the permanent set strain (ca. 1.0), (C) during extension at strains larger than the permanent set strain, and (D) during retraction to zero stress.

at a strain about 1.0. Diagram C indicates that at higher strains (>1.0) all lamellae (the residual of the original crystallites and the strain-induced crystallites) are aligned with their normals parallel to the stretching direction. In addition, a large fraction of the amorphous chain segments are also oriented along the stretching direction, storing the entropic recovery force. Diagram D indicates that upon complete retraction back to zero stress the permanent set crystalline network structure persists, where the network lamellar stacks change slightly with respect to the fully stretched lamellar structure. The relaxed lamellar stacks have a smaller average long spacing and preferred orientation having their normals tilted against the original stretching direction.

In the second cycle, the residual crystalline network structure (diagram D), as being permanent set, exhibits an ideal elastic behavior similar to that of cross-linked rubbers. Crystalline lamellar stacks behave as the cross-link points. During extension, the structure of lamellar stacks changes slightly, i.e., the long period increases and the lamellar normals become parallel to the stretching direction (diagram C), but the connecting amorphous chain segments between the stacks can get stretched and oriented, forming new crystallites of even thinner thickness. The addition of new strain-induced crystallites would increase the network density, resulting in a rapid stress upturn. The combined mechanisms of the increase in the network density and the deformation of non-Gaussian amorphous chain segments between the network points (lamellar stacks) enable the TPE after permanent set to behave as vulcanized rubber. Similar to rubber, the strain-induced crystallites in the framework of the permanent set lamellar structure are not thermally stable, such that they melt away at room temperature upon relaxation because of the increase in entropy.[19] At zero stress, the permanent set lamellar network recovers completely, even though the network structure changes into a tilted arrangement with more compact stacking (decreasing long period).

Conclusions

In this study, combined SAXS and WAXD results indicate the tensile deformation in the first cycle can induce a permanent set lamellar network structure. Some concluding remarks from this work are summarized as follows.

1. During extension of a melt-pressed propylene-based EP copolymer (84.3 wt % of propylene content), a fraction of crystallites in the form of randomly oriented folded chain

lamellae is destroyed and the rest reoriented even at low strains. At strain 1.0, an oriented lamellar network structure forms, containing strain-induced lamellae and reoriented residual lamellae with their normals parallel to the stretching direction. This network structure exhibits permanent set properties.

2. The network points are lamellar stacks thermally stable at room temperature, but they are compliable with stress. At low stress (e.g., during extension at low strains or during retraction), the lamellae in the stacks become tilted and close packed; at high stress (during extension at high strains), the lamellar normals become parallel to the stretching direction and the lamellae are more separated.

3. At strains larger than 1.0, further strain-induced crystallization takes place in the framework of the permanent set lamellar structure. However, these crystals are not thermally stable (probably very defective) at room temperature and melt away upon relaxation. The process of strain-induced crystallization increases the network point density and enhances the stretching of non-Gaussian amorphous chains between the network points, resulting in a rapid strain-hardening response.

4. The permanent set lamellar structure behaves as a cross-linked rubber with no yield stress but enhanced strain-hardening behavior. The stress−strain curves and the in-situ structure development are completely reversible in the higher ordered cyclic deformation.

Acknowledgment. We acknowledge the assistance of Dr. C. A. Avila-Orta for synchrotron SAXS and WAXD experimental setup. The financial support of this work was provided by the NSF (DMR-0405432).

References and Notes

(1) Yang, Y.; Chiba, T.; Saito, H.; Inoue, T. *Polymer* **1998**, *39*, 3365.
(2) Liu, L.; Hsiao, B. S.; Fu, B. X.; Ran, S.; Toki, S.; Chu, B.; Tsou, A. H.; Agarwal, P. K. *Macromolecules* **2003**, *36*, 1920.
(3) Datta, S.; Srinivas, S.; Cheng, C. Y.; Hu, W.; Tsou, A.; Lohse, D. J. ACS Rubber Division Fall Meeting, 2003, paper #60.
(4) Dharmarajan, N.; Williams, M. G.; Datta, S. ACS Rubber Division Fall Meeting, 2003, paper #58.
(5) Toki, S.; Sics, I.; Liu, L.; Hsiao, B. S.; Tsou, A. H.; Datta, S. ACS Rubber Division Fall Meeting, 2003, paper #59.
(6) Guerra, G.; de Ballesteros, O. R.; Venditto, V.; Galimberti, M.; Sartori, F.; Pucciarello, R. *J. Polym. Sci., Part B: Polym. Phys.* **1999**, *37*, 1095.
(7) Kolbert, A. C.; Didier, J. G.; Xu, L. *Macromolecules* **1996**, *29*, 8591.
(8) Mathot, V. B. F.; Scherrenberg, R. L.; Pijipers, M. F. J.; Bras, W. *J. Therm. Anal.* **1996**, *46*, 681.
(9) Hong, K.; Strobl, G. *Macromolecules*, in press.
(10) Estes, G. M.; Cooper, S. L.; Tobolsky, A. V. *J. Macromol. Sci., Rev. Macromol. Chem.* **1970**, *4*, 313.
(11) Bonart, R. *J. Macromol. Sci., Phys.* **1968**, *B2*, 115.
(12) Koberstein, J. T.; Gancarz, I. *J. Polym. Sci., Polym. Phys.* **1986**, *24*, 2487.
(13) Yeh, F.; Hsiao, B. S.; Sauer, B. B.; Michel, S.; Siesler, H. W. *Macromolecules* **2003**, *36*, 1940.
(14) Ran, S.; Fang, D.; Zong, S.; Hsiao, B. S.; Chu, B.; Cunniff, P. M. *Polymer* **2000**, *42*, 1601.
(15) Fraser, R. D. B.; Marae, T. P.; Miller, A.; Rowlands, R. J. *J. Appl. Crystallogr.* **1976**, *9*, 81.
(16) Somani, R. H.; Hsiao, B. S.; Nogales, A.; Fruitwala, H.; Srinivas, S.; Tsou, A. H. *Macromolecules* **2001**, *34*, 5902.
(17) Yang, W.; Li, B. H.; Feng, J.-M.; Shi, W.; Yang, M.-B. *J. Appl. Polym. Sci.* **2003**, *89*, 686.
(18) Lamberti, G.; Brucato, V. *J. Polym. Sci., Part B: Polym. Phys.* **2003**, *41*, 998.
(19) Toki, S.; Sics, I.; Ran, S.; Liu, L.; Hsiao, B. S.; Murakami, S.; Senoo, K.; Kohjiya, S. *Macromolecules* **2002**, *35*, 6578.
(20) Toki, S.; Hsiao, B. S. *Macromolecules* **2003**, *36*, 5915.
(21) Toki, S.; Sics, I.; Ran, S.; Liu, L.; Hsiao, B. S.; Murakami, S.; Senoo, K.; Kohjiya, S. *Polymer* **2003**, *44*, 6003.
(22) Bonart, R.; Hosemann, R. *Kolloid Z. Z. Polym.* **1962**, *186*, 16.
(23) Yeh, F.; Hsiao, B. S.; Sauer, B. B.; Michel, S.; Siesler, H. W. *Macromolecules* **2003**, *36*, 1940.
(24) Ajji, A.; Guevremont, J.; Cole, K. C.; Dumulin, M. M. *Polymer* **1996**, *37*, 3707.

MA0600106